Astronomy & Astrophysics manuscript no. paper˙v˙9
March 2, 2012
© ESO 2012

Comparing methods to remove scattered light in earthshine data: New telescope, New methods

P. A. Thejll, C. Flynn[2], H. Gleisner[1], Torben Andersen[3], Ahmad Darudi[3,4], Mette Owner-Petersen[3], Henriette Schwarz[3,1], and Jacob Weismann Poulsen[,1]

(Affiliations can be found after the references)

Received September 15, 1996; accepted March 16, 1997

ABSTRACT

Context. Observations of earthshine can be used to determine the terrestrial albedo, which is of importance for climate studies, and as a potential source of calibration data for short wavelength satellite radiance experiments. However, determination of terrestrial albedo in this way requires removal of the scattered moonlight from the bright side that interferes with that of the dark side.
Aims. We describe a new instrument for measurement of earthshine. We evaluate existing methods for removing scattered light as well as a family of new methods in a setting where synthetic lunar images are used, and we present some first results from our facility..
Methods. Direct imaging allows recording the intensities of the earthshine and the moonshine with common-mode rejection of some sources of interference. Forward modelling of the images are based on an empirically determined generic PSF that is adapted to nightly conditions; estimates of the earthshine intensity, or terrestrial albedo directly, are then based on analysis of corrected images or directly on the best-fitting ideal model image.
Results. We present a new earthshine telescope, now in operation at Mauna Loa Observatory, Hawaii. First results are presented and reduced with several methods and compared. We confirm that the traditional linear extrapolation method for scattered-light removal can achieve precisions at the 1% level, but is limited in accuracy by the presence of scattered-light remnants. Some improvement of this method is demonstrated by use of logarithmic images instead of linear intensity images. However, the new methods we introduce are shown to potentially offer accuracies and precisions in the 0.1% range by co-addition of many short-exposure images, for a range of lunar phases up to about 100 degrees from New Moon. On data from two nights of observing we find significantly better performance in a forward-modelling method than in a standard method, while results do not yet reach the potential suggested by the theoretical study.
Conclusions. The new method offers significant enhancements for extraction of albedo or albedo-related data from images, future and archival, of the Moon.

Key words. lunar photometry – terrestrial albedo – data analysis – observing techniques

1. Introduction

Terrestrial albedo is a key factor in Earth's radiative balance and thus in climate research. Albedo changes as the climate system changes – cloudiness, land-use changes, extent of ice and snow on sea and land, whitecaps on windy oceans, biological activity, aerosol load and so on all depend on the state of the climate system - but induced changes in albedo may also *cause* climate change. Simple energy-balance model considerations suggest that a 1% change in albedo is roughly equivalent to a mean global temperature change of 0.5 K. Feedback processes in the climate system are certainly expected to modify that simplistic picture: but it is evident that precision of the terrestrial albedo data in the sub-1% range is required to empirically consider the role of albedo in climate change - whether passive or active.

Prior to the satellite era, knowledge on the terrestrial albedo was very uncertain and not until the first space-based determinations of the Earth's radiation budget – those of the Nimbus-6 and 7 satellites – was it firmly established that values of the albedo at short wavelengths is close to 0.3 (Stephens et al. 1981). The result was based on measurements from satellites in low-Earth orbit, which were hampered by temporal sampling problems. Since then, such observations have been supplemented by observations from geostationary orbit. While the instruments on Earth observing satellites have gained in sophistication and precision, the GERB instrument of the geostationary MSG2 satellites is only required to be 1% accurate at visual wavelengths following laboratory calibrations (Johannes & Mueller 1997). Once in space calibration is based on observation of terrestrial reference surfaces (e.g. salt lakes) or the Moon. In the latter case the Moon is imaged from the satellite and calibrated against a database of lunar irradiance values for different phases of the Moon (Stone 2008). In principle, it should thus be possible to maintain instrument accuracies in the short wavelengths near the 1% level, while precision is better than that.

An alternative method, complementary to current satellite based observational systems, is to measure the ratio of the intensity of the Moon's dark side (DS; illuminated only by earthshine) to that of the bright side (BS; illuminated also by sunshine). The BS intensity is proportional to the solar irradiance while the DS intensity is proportional to the fraction of the solar irradiance reflected off the Earth in the direction of the Moon. Hence, the BS to DS ratio is proportional to Earth's albedo, where the proportionality constant depends only on geometry and factors related to the reflective properties of the Moon. To acquire global albedo information from lunar observations a global network of automated Moon telescopes is needed. At present at least four of these instruments exists – one at Big Bear Solar Observatory in California, one on Tenerife in the Canary islands and one in Crimea (Goode et al. 2010) and now ours at the Mauna Loa Observatory on Hawaii. Additional instruments

are needed further East at longitudes corresponding to Eastern Asia or Australia.

The relative-photometry method described above incorporates *common-mode rejection* of some of the factors that confound absolute-intensity observations: effects of time-varying atmospheric transparency, instrument sensitivity variability, and variations of the solar irradiance. It has been suggested (Goode et al. (2001) and Pallé et al. (2009)) that such albedo observations can potentially reach higher precision than traditional satellite based observations. However, the advantages of common-mode rejection only applies to those effects – instrumental or atmospheric – that remove photons from the path. Scattering of photons from the BS into the DS on the imaging device still gives rise to errors. Hence, the main technological challenge involved in designing equipment for this type of measurements is to minimize the amount of scattered light, and one of the major challenges in the photometric analysis of the images is to properly remove the effects of the remaining light.

In this paper, we present the new instrument, first results, and discuss methods for removing scattered light in earthshine (ES) observations. We then test existing and new methods with synthetic lunar image data, by generating realistic simulated observational data, and reducing it for scattered light. We then extract ES intensities, or terrestrial albedo directly, and compare these to the known values.

2. Instrument

Our instrument is based on the principle presented in Qiu et al. (2003) (their Figure A1). It is essentially a small refractor with specialized occulting devices fitted in the ray path (Darudi et al. 2010, figure 1). Details of the basic optical design and test-bench performance of our telescope have been given elsewhere (Owner-Petersen et al. 2008) but the instrument is, briefly, a refractor with a 30 mm objective and focal ratio of 12.5. We extend the Big Bear Solar Observatory (BBSO) concept by providing for four ways of observing the Moon. In the prime focus, a device is able to insert *either* an internal occulting device - a solid knife edge with a straight edge and position it to match the cusp angle of the Moon and thus cover the bright side of the Moon during dark side observations, *or* a knife edge-shaped semi-transparent set of neutral density filters - to enable simultaneous observation of the dark and bright side of the Moon. The direct imaging mode is the simplest and we base this paper on that system - the other observing modes will be analysed and discussed in future work. A collimating lens produces a collimated beam in which a Lyot stop and two filter wheels are situated. One carries Johnson B and V filters along with two red filters picked to delineate a spectral feature in the reflectivity of vegetation near 750nm, and a third 'white light' filter which is the same IR-cutting filter as used in the BBSO instruments, to enable an observing mode identical to theirs (Goode et al. 2010). The second filter wheel in the collimated beam carries a set of neutral density filters. Placing the filters in the collimated light reduces the influence of the spatial homogeneity of the filters. A summary of the intended observing modes is given in table 1.

A second lens focuses the image on the CCD, which is an ANDOR iXon-897BV with a back-illuminated, thinned and non-coated 512×512 chip with pixel size 16μm. The CCD is operated in standard amplification mode - i.e. the special EM mode is not utilized.

The CCD camera has a thermostatic temperature control and it was evident after some initial testing that a 20-minute cycle in bias with amplitude of roughly $1/2$ count is present. To remove this bias it is necessary to take dark frames just before and after each science image.

The telescope was installed on Mauna Loa at the NOAA geophysical observatory there (altitude 3397 m) in March 2011, and is operated remotely and semi-automatically.

3. The Point Spread Function

Central to efforts for removing bright-side scattered light on the dark side is an understanding of the combined atmosphere/instrument point spread function (PSF), and methods for correction. Joint atmospheric/instrumental PSF have been discussed at least since de Vaucouleurs (1948),de Vaucouleurs (1958) and King (1971) reported on the power-law nature of the PSF in various types of astronomical images. Racine (1996) considered the PSF from a less empirical point of view, while Bernstein (2007) summarized the power laws determined by investigators until then.

Scattered light from a point source is typically described by the Point Spread Function (PSF), most commonly as the 1-D (i.e. azimuthally averaged) profile of the intensity as a function of radius. Very careful photometry may require that the PSF be specified in 2-D and may also be parameterised because of variation across the field of view imaged by the CCD. Stars are of course point sources, and measuring the profile of isolated bright stars is the usual procedure to determine the PSF, and this can be routinely achieved with astronomical images to a few times the Full Width Half Maximum (FWHM) of the stars. We are interested in the PSF out to much larger distances – to the edge of the field of view of the telescope (i.e. of order a degree). We have measured the PSF on these scales using bright stars, and the Moon itself.

In a telescope unaffected by both atmospheric effects and telescope aberrations, the PSF is set by diffraction. The PSF is then given by $(J_1(x)/x)^2$ where $x \sim rD/F$, r is the angle from center of the PSF, D is the telescope diameter and F is the focal length. The asymptotic behaviour of the first-order Bessel function of the first kind, J_1, is such that the envelope of the PSF in a non-monochromatic observation goes as $1/r^3$. Our telescope, however, is not limited by diffraction, but by chromatic and geometric aberrations (Darudi et al. 2010). For large aperture telescopes, that is $D/r_0 \gg 1$, where r_0 is Frieds parameter (the atmospheric correlation length), the considerations in Racine (1996) lead to an expectation of $1/r^2$ behaviour in the PSF. As our telescope is installed at Mauna Loa, which is a good site, we expect that r_0 is 20–40 cm at night and so, given an objective diameter of 3 cm we certainly have $D/r_0 \ll 1$ and the PSF cannot be simply estimated. We must determine it experimentally, and have found that it is possible to scale an empirically determined PSF to night conditions by exponentiating the empirical PSF.

In order to accurately measure the luminosity of the earthsine (ES) side of the Moon, we need to understand very well how light scatters from the bright side (BS).

Several hundred images of the bright star Altair ($V = 0.8$) were taken in October 2011, using short exposures so that the center of the star was well exposed (circa 55,000 counts/pixel), using an exposure time of 40 ms. The exposures were bias subtracted, aligned carefully on Altair and coadded. The FWHM of the image obtained is approximately 3 pixels (or 21 arc seconds at the image scale of 7 arc seconds per pixel). The radial profile is shown in Figure 1 on a log-log scale, and shows an approximately Gaussian core within a power-law halo, which extends to $r \approx 30$ pixels (210 arc seconds, or 3.5 arc min). Beyond the Gaussian core, the halo shows the classic power-law seen in all

Table 1. New Earthshine telescope observing methods.

Method name	Description	Comment
Co-Add	Short exposures of the whole Moon, so that BS is not overexposed. DS just visible - typically hundreds of images are aligned and averaged using outlier rejection.	Only realistic at lunar phases near New Moon. Independent of shutter precision. Common modes are rejected.
BBSO	Short exposures of the BS. Then BS is covered by occulting blade and longer exposures of DS are taken.	For BS exposure precise knowledge of exposure time required. Some common modes not rejected.
Modified BBSO	Same as BBSO mode but the short exposure is taken through a neutral density filter.	ND filter density required to avoid bias, but precision is good. Dependence on knowing the shutter speed is reduced. Some common modes not rejected.
Lund	Whole Moon imaged through a semi-transparent occulter. The DS is seen through the transparent part of the device while the BS is reduced in intensity by a semi-transparent reflecting film of deposited metal. Several densities provided in order to accommodate observations at different lunar phases.	Density of semi-transparent blade required to avoid bias. Common modes rejected.

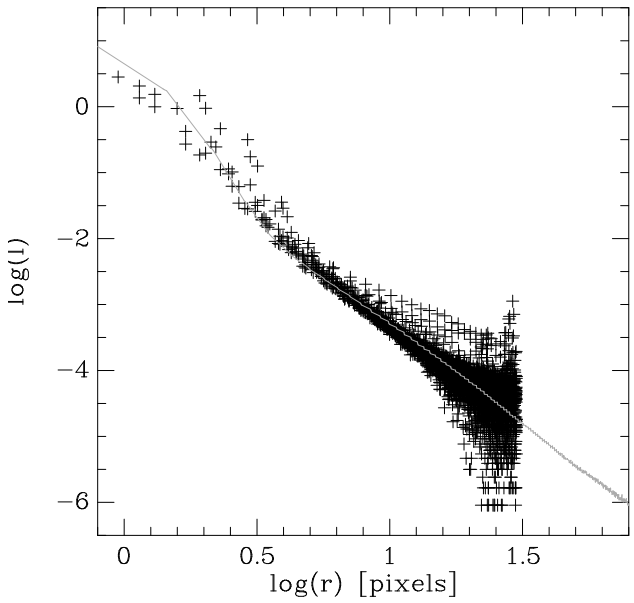

Fig. 1. The point spread function determined on an excellent night using hundreds of images of the star Altair. The grey line shows the composite PSF adopted in this work, here modelled so that the wings have slope -3. A 'spur' on the PSF in one direction parallel to the rows of the image causes the cloud of points at large radius above the dense sequence formed by the other points. The origin of the spur is unknown but is not in the read-out direction of the image, and we tentatively conclude it is a slight optical artefact caused by some internal reflection. The spur is not modelled as part of the system PSF at the moment.

other studies of this type, and detaches from the core at approximately $\log(r) = 0.5$ (3 pixels, 21 arcsec). The slope of the power-law beyond this point is -3.0 out to $\log(r) = 1.3$ (20 pixels, ≈ 2 min), beyond which the flux becomes unreliable, because the halo merges with the background.

We are interested in characterising the PSF out to the edge of the field of view, approximately a degree of arc, very much further than this stellar profile reaches. This can only be achieved with our images of the Moon itself. To simplify things we used short exposure (20 ms) images of the full Moon, also exposed to have about 55,000 counts/pixel at their brightest point. Trial PSFs were constructed by taking the stellar PSF $f(r)$ of Figure 1, and extending the power-law halo outward, but allowing the slope of the power law, α to remain a free parameter $\mathrm{PSF(r)} \propto f(r)^{\alpha}$.

The inner, Gaussian-like core of the PSF is also exponentiated under this assumption but is so close to the center of the star that the effect on the final fitting is negligible – the intention is to describe the slope of the stellar halo.

A synthetic image of the Moon at the same phase and rendered at exactly the same pixel scale was created, and convolved with trial PSFs for a range of α, and compared to the observational data. The convolution was done using 2-D FFTs of the synthetic Moon placed into the center of an image 3 times larger than the 512×512 CCD size, since scattered light of the Lunar BS can be significant at the edge of the frame, and edge-wrapping effects must be suppressed. This proved a very effective procedure.

We were able to fit the scattered light out to the edges of the frame very well, with uncertainty in the value of the fitted α of just 0.01. We find that the halo slope can vary considerably from night to night, with a range of α from about -2.9 to -2.7 on nights which are completely clear, to -2.5 under conditions of very thin cirrus cover (as revealed by the Allsky camera at Mauna Loa) to < -2 under light haze or otherwise poor sky conditions.

We have observed bright stars, Jupiter and the Moon in all filters on the system and for a wide range of sky conditions and Lunar zenith angles (all determinations of α were made close to the zenith for stars and Jupiter). From sequential exposures, the filters can be seen to produce slightly different halo power-law slopes of both stars and the Moon itself, but the main effect on the slope is the sky condition. In the longer term, the condition of the optics may change and affect α: this should be straightforward to pick up as we need to fit α to every Lunar frame as part of the ES measurement.

Since the Moon is an extended object the aureole profile is not the same as the PSF profile - except at large distances from the Moon. The empirical power-law dominated halo exponentiated is also a power-law with an effective exponent equal to the product of the empirical slope and the imposed exponent. We do not suggest that the empirical basis-halo must be determined nightly, but it would be a possibility, and is necessary if the accumulation of dust, or micro-scratching of the objective lens, causes a gradual change in the underlying optical performance.

4. Methods and Synthetic data

Several methods for reducing lunar observations to ES intensity data, or directly into terrestrial albedo estimates will be discussed. The image a telescope records is corrupted by counting-statistics noise and several 'smearing' effects have been added by the atmosphere and the optics. The CCD also leaves its own fingerprint in the data. In the present paper we are mainly focusing on the combined atmosphere-optics system having an effective PSF that scatters bright light from the BS to the DS.

By extinction light is spread by scattering but also removed (to a smaller extent for visual wavelengths) by absorption. The absorption affects all pixels in the same way, apart from the slightly higher extinction at the lower edge of an image compared to the top of the image. However, scattering has two effects: Light is removed from bright areas and spread over nearby regions. If the light is mainly spread in a region of almost equal brightness (such as the BS) mainly a slight blurring effect is seen, while if the light is spread across a dark region then the intensity there is falsely increased.

We first discuss our method for constructing synthetic lunar images. Then we discuss the existing and two new methods for removing scattered light from images of the Moon. The new methods are based on a forward modelling paradigm.

4.1. Synthetic lunar images

Synthetic lunar images are used for assessment of the methods for removing scattered light in the images. These synthetic images are produced by a *lunar radiance model* that simulates the appearance of the Moon in a CCD image. The model accounts for the viewing geometry and uses broad-band bi-directional reflection functions (BRDFs) to describe how sunshine is scattered off the lunar surface. The scattering properties depend on the selenographic latitude and longitude – i.e. location on the Moon – and account for the different reflection properties of the lunar maria and highland regions. The result of the simulation is an 'ideal' image of the Moon unaffected by scattering of light in the atmosphere or instrument.

The components of the lunar radiance model are:

- a geometrical description of the Earth-Moon-observer system
- a photometric description of the lunar light-scattering properties
- a simplistic photometric description of the terrestrial light-scattering properties
- an algorithm to ray-trace from the individual CCD pixels to the surface on the Moon

The geometrical description is taken from an ephemeris describing the positions and rotations of Earth and Moon as a function of time. The geometric description includes the observer's position, the lunar librations, and the distance and direction of the Sun from the Earth-Moon system.

The BRDFs describe the probability that an incident photon is scattered in a certain direction as a function of angle of incidence, angle of reflection, and phase angle. The formulation of the BRDF follows Hapke (1963) and Hapke (1993), and the BRDF is normalized to give an albedo roughly similar to that measured in the 750 nm band by the UV/VIS camera on-board the Clementine mission (Robinson & Riner 2005).

The role of the model Earth in the present setup is to illuminate the Moon with ES. The illumination must be of the right order of magnitude for the DS to BS intensity ratio to be realistic. This can be accomplished by a simple Lambertian sphere Earth-model with a uniform single-scattering albedo (SSA). To generate temporal albedo variations, an optional Earth albedo model incorporating land, ice, and ocean reflections, and a realistic cloud distribution, is available (Ford et al. 2001). Manalo-Smith et al. (1998) provide other empirical terrestrial BRDFs.

The lunar images are produced by a simple form of ray tracing. Each pixel on the imaging device collects light from a certain solid angle in a certain direction. This direction is traced to the surface of the Moon. From the computed selenographic latitude and longitude, and knowing the angle of incidence of the sunshine and ES, and the phase angle at the Moon, we can compute the light scattered in the direction of the observer. This is done for each individual pixel leading to the buildup of an image. An advantage of this simple ray-tracing algorithm is that it gives the correct stereo-graphic projection as a result of the finite Moon-observer distance, without explicitly computing the projection effects. Scene models where the Earth is rendered have been described, for realistic image rendering purposes in the animated-motion picture industry (Jensen et al. 2001), for exoplanet investigations (Oakley & Cash 2009) and recently (Yu et al. 2011) for a space-based ES instrument.

4.2. The LINEAR sky-extrapolation method

The BBSO group performing observations of ES (Goode et al. 2001) pioneered a method for compensating for scattered light in images of the Moon based on linear extrapolation of the scattered light intensity on the sky. It was noticed that the intensity follows an almost linear dependency on the distance to the lunar disc centre: with a regression estimating the relationship between intensity and radial distance a method was devised for extrapolating onto the lunar disc and subtracting scattered light there. The BBSO group applies that method to images taken with the BS covered by an occulter inside the telescope, allowing for long exposure times and large signal to noise ratios (SNRs) on the DS disc without suffering from the consequences of a massively overexposed BS or the effects of intense light reaching the CCD detector and reflecting off its front surface and scattering detrimentally inside the telescope.

From the outset we wanted to first test the simplest observing mode on our telescope and have explored direct imaging and how to use a large number of images - each exposed well enough to avoid overexposure of the BS. By aligning them and averaging we improve the SNR ratio on the DS without overexposing the BS. We will evaluate, using synthetic data, the properties of the existing method on co-added images we construct from large numbers of short exposures to obtain a high SNR.

Calling the above method 'LINEAR' from now on, we will also consider the 'LOGARITHMIC' method: It is the same as LINEAR but works on logarithmic intensity scale.

4.3. The empirical forward method - EFM

Our two forward modelling methods are based on numerically replicating the process that causes the Moon to be recorded as a blurred and noisy object. After a replica image has been fitted it can be compared to or subtracted from the observed image and yield information.

In the Empirical Forward Model (EFM) we use the sky part of the observed image as a model of the source of the scattered light. Convolving that spatial source with trial flux-conserving

PSFs we can iteratively adjust model parameters in the PSF until a good match is found between the sky part of the observed image and trial synthetic images. By choosing only the sunlit part of the Moon as the source, the difference between the observed image and the best fitting model will be a measure of the required DS intensities outside the atmosphere.

The choices of which part of the image to use as source and which part to use for model fitting influences the results, so testing is in order - and we do so based on synthetic lunar images where the DS intensity is known. As source we choose that part of the observed image where the intensity is above some fixed fraction of the maximum intensity - e.g. 1/75th. This is an arbitrary choice so we experiment to see which value gives good results - setting it too low means that the DS is being included in the model of the source which implies that that part will be removed at the subtraction stage - as the DS increases in relative intensity as the New Moon is approached the choice of the cut-off sets which part of the lunar cycle you can access with the method.

We have found that the difference between modelling the BS source as those pixels with intensity above one 75th of the maximum BS intensity on the one hand, and modelling the source as all pixels that are sun-lit on the other, corresponds to a difference in the halo intensity at the DS reference patch of from 0.01 percent up to a few tenths of a percent, when the resulting model halos are normalized to the same value at maximum. The influence of the choice of source model is even less when we consider the effect of subtracting the *best-fitting* halo, and we shall use the 1/75 rule for building the model source from now on.

We fit the EFM to the sky around the lunar disc, or parts thereof: The minimization requires adjusting three parameters - one equivalent to requiring flux conservation, one equivalent to a pedestal or offset in the image and one parameter adjusting the width of the PSF. These can be found by using a conventional numerical minimization, or in a grid search with sufficiently small steps. Typically, the image scaling parameter is linked to the choice of the others and can be found algebraically.

We chose the grid search method due to its obvious parallelisation potential. Our ultimate goal was to be able to process 50.000 images within a few hours using supercomputers. Beforehand though, we found that a solid understanding of the underlying accuracy of the algorithm or rather it's potential implementation was extremely important to us. We approached this study by doing various implementations of the algorithm (serial, parallel at the α step level and parallel at the pixed level) in various languages (`c`, `c++/stl`, `cudac++/thrust`) and eventually ran the binaries on various hardware platforms (cray XT5, cray XE6 and nvidia tesla GPU). Each implementation was done using both 32bit precision and 64bit precision. The implementations as well as the results of this study are available upon requests.

The forward modelling involves the convolution of images with extended PSFs - this is done by multiplication in the frequency domain followed by inverse transformation. Since the PSFs have extended wings we need to 'pad' the images to avoid edge-effects during the FFT based folding - we have found it sufficient to lay them out in a 3×3 grid of same-size empty images. A *brute-force* direct convolution appears an attractive alternative as the padding is then not needed, but is quite a lot more computationally intensive (hours vs minutes).

4.4. The full forward method - FFM

The above EFM method yields scattered-light corrected information on the intensity of the DS. Such data still need to be further reduced to yield terrestrial albedo information, as is done by the BBSO team (e.g Qiu et al. 2003). As an alternative, we introduce here the full forward model ('FFM') method in which a model of the Earth and its reflective properties is allowed to set the ES intensity - in this way the various reduction steps used for inverting conventionally observed ES are subsumed into the modelling of the reflection of light at the Earth; a best fitting model is determined and directly yields an estimate of the terrestrial albedo. The fitting of this model to the observations is done on sky as well as on the lunar disc: Again we have two parameters that correspond to flux conservation and matching the sky level, and a third parameter still describes the PSF, but now in addition we have several other parameters or model-choices that can be determined - these describe the terrestrial albedo model.

We present a test of the FFM next, based on synthetic images incorporating an offset, a scaling, a width parameter for the PSF and a terrestrial albedo. The synthetic images are calculated with the system described in section 4.1, and appropriate amounts of Poisson noise is introduced. The test proceeds by setting up a series of synthetic images and two auxiliary images for the same phases but where one has been calculated for albedo 0.0 and the other for albedo 1.0. By scaling these two images linearly we enable a non-linear least squares minimization method – MPFIT2DFUN (Markwardt 2009) – to not only find the offset and the PSF parameter, but also, directly, the terrestrial albedo. The image factor is found by imposing flux-conservation between the synthetic realistic image and the fitting routines trial images which depend on the offset, the PSF parameter and the synthetic image illumination (i.e. the ES). The method is set up to minimize the relative root mean square error (RMSE) over the entire image - sky and lunar disc, BS and DS. Individual pixel weights are based on $\frac{1}{\sigma}$ where σ is given by Poisson statistics.

5. Results from tests on synthetic images

About a month's worth of realistic but synthetic images were generated at 9 hour intervals, resulting in 83 images, in order to represent all observing conditions. Each of these were made with realistic levels of Poisson noise and blurring, and a realistic maximum exposure level of 55000. The blurring was performed using a power-law PSF based on an empirical profile extended linearly in log-log space; this PSF was then raised to a fixed power. The combined effect of using the empirical power-law and the exponentiation was that of a power law with power near -2.9, corresponding to a clear night with most of the PSF due to telescopic elements.

The images were produced in two sets - one consisting of 83 single images and the other consisting of averages of 100 images, to simulate the effect of the CoAdd method. Each of the images in each set were reduced for scattered light using the above methods.

5.1. Results of the LINEAR and LOGARITHMIC methods

We implemented the LINEAR method by closely following Qiu et al. (2003). We tested whether a linear least squares or a least absolute deviation regression works best - very little difference was found. We use the least squares method here because that choice enables a simple evaluation of the goodness of fit. When the regression was deemed 'good' by the formal quality of the

fit it was used to extrapolate the regression onto the lunar disc all the way to the disc centre and the extrapolated light subtracted inside the relevant cone. We noted that the data are a little inter-dependent - the estimates of the errors on the data enter into the estimation of the goodness of fit as does the number of points, but few of the regressions seemed to test out as being good - the required p level was rarely reached. We overcame this problem by lowering the parameter that gives the number of independent points from the actual number of points to one third of that: this is consistent with some moderate degree of serial correlation in the residuals - perhaps due to the halo not being quite linear after all, and some curvature noted near the disc rim.

After cleaning the images the DS intensity was extracted from 21×21 pixel patches situated at 2/3rds and 4/5ths of the radius from the disc centre at the same row as the center of gravity of the light, on the DS. The same boxes were measured in the known synthetic images, and the two values compared. Figure 2 shows the results as a function of lunar phase. Note that it is in practise very difficult to observe the Moon for any length of time at lunar phases below about 30 degrees - the proximity to the Sun set the limit,

We see that results with small errors are available only for a narrow range of lunar phases - e.g. less than 40 or 50 degrees. Only for α=-2.88 and high SNR can the methods reach up to phases of 60 or 70 degrees. We see in general that the LOGARITHMIC method is somewhat better than the LINEAR, and that best results are found close to the rim, as expected. We also see an asymmetry - as the lunar phase passed Half Moon the analysis switched to the other side of the lunar disc where and area of different lunar albedo was in the box. These results suggest that application of the LOGARITHMIC method can contribute to better scattered-light removal in the sky-extrapolation framework. In addition, we note the prevalence of a strong bias - for large lunar phases both linear and logarithmic images have increasing levels of residual scattered light with increasing lunar phase.

5.2. Results from the EFM method

Figure 3 shows results from the test of the EFM method. Two values of α were used, and stacks of 100 images were simulated. We see that for a narrow PSF (α=-2.88) it is possible to determine the DS intensity to better than 1% for lunar phases out to about 100 degrees from New Moon, but that for broader PSFs (ie on lower-quality nights) the error in DS determination is generally at the several-percent level. The Figure shows absolute values of errors for display purposes: There was little bias in the α=-2.88 results with errors scattered around 0, while bias was present for the α=-2.56 case - most errors had the same sign.

5.3. Results from the FFM method

Figure 4 shows the results for the FFM - we extract the terrestrial albedo directly (shown), as well as the sky offset, flux factor and α (not shown). For single images results are within ±0.2% from the known value for lunar phases up to 60 to 80 degrees, depending on the PSF width. Bias, is present but small. When 100 images are coadded the method improves markedly - bias is almost gone and acceptable results are obtained for phases up to ±110 degrees. Due to issues related to difficulties in realistically estimating the number of degrees of freedom in the data we do not show the fitting methods' formal estimates of uncertainties, as these are probably underestimated. Instead we estimate the errors using Monte Carlo simulations. One standard deviation intervals for the fits are estimated by performing Monte Carlo simulations at two characteristic lunar phases: The fit was estimated 100 times using new realizations of the Poisson noise - this gives a distribution in the fitted albedo, for instance, which can be used to realistically discuss the errors on the FFM as a function of lunar phase. Table 2 shows the results.

Table 2. Estimates of FFM method fitting error on albedo, from Monte Carlo simulations and synthetic lunar images. For two lunar phases and two choices of the number of images to stack, 100 Monte Carlo realizations of the Poisson noise in the synthetic image were produced and the best fitting FFM model found for each. The resulting 100 values of the albedo were placed in a histogram and the standard deviation and the median value bias extracted. Lunar phase is 0 at New Moon. Emphasized with bold are cases where both uncertainty and accuracy is better than 0.1&.

Lunar phase	No. of im.	α	Δalbedo	Median bias
-36.7	1	-2.56	0.122%	-0.225%
-36.7	100	-2.56	**0.013**%	**0.049**%
-36.7	1	-2.88	0.098%	-0.178%
-36.7	100	-2.88	**0.0**%	**0.058**%
86.1	1	-2.56	0.66 %	-0.59%
86.1	100	-2.56	**0.08**%	**0.010**%
86.1	1	-2.88	0.37 %	-0.34%
86.1	100	-2.88	**0.04**%	**0.012**%

Table 3. Observing nights discussed in this paper- Lunar phase is counted from New Moon. Sky conditions were visually estimated from the all-sky camera available at MLO.

JD	Lunar phase	Notes
2455858	44	Moon rising, clear - dry
2455917	41.5	Moon rising, very slight haze - dry

6. Results from observations

Since mid-2011 we have been observing the Moon from MLO regularly on favourable nights when weather and lunar phase permitted. The weather conditions are generally good at MLO with few clouds, but December 2011 was quite wet and cloudy. We show first multi-band observations in this paper from the nights of JD 2455858 and 2455917 (see Table 3 for details on observing conditions). Only results from the direct imaging mode will be discussed here. In this mode hundreds of images are obtained for each filter, along with dark frames. The dark current in the camera is extremely low (0.0002 e^-/pix/s, when cooling is on) and for the short exposure times we use there is negligible difference between bias and dark frames - but dark frames of the same exposure time as the observation (typically a fraction of a second) were obtained before and after each multi-image sequence, thus making it possible to compensate for the time-dependent bias. Flat fields have been obtained from the dusk sky, and from a hohlraum lamp mounted in the observatory dome.

After the usual bias subtraction and flat-fielding, the images were aligned and averaged and analyzed. Alignment was performed using the correlation-based method of Chae (2004). We find it is possible to align images to approximately the 0.1 pixel level, which is adequate for our purposes. Some of the alignments fail due to the automatic method for finding lunar disc centre and the lunar rim - which is necessary in order to align frames. These failed alignments reduce the number of

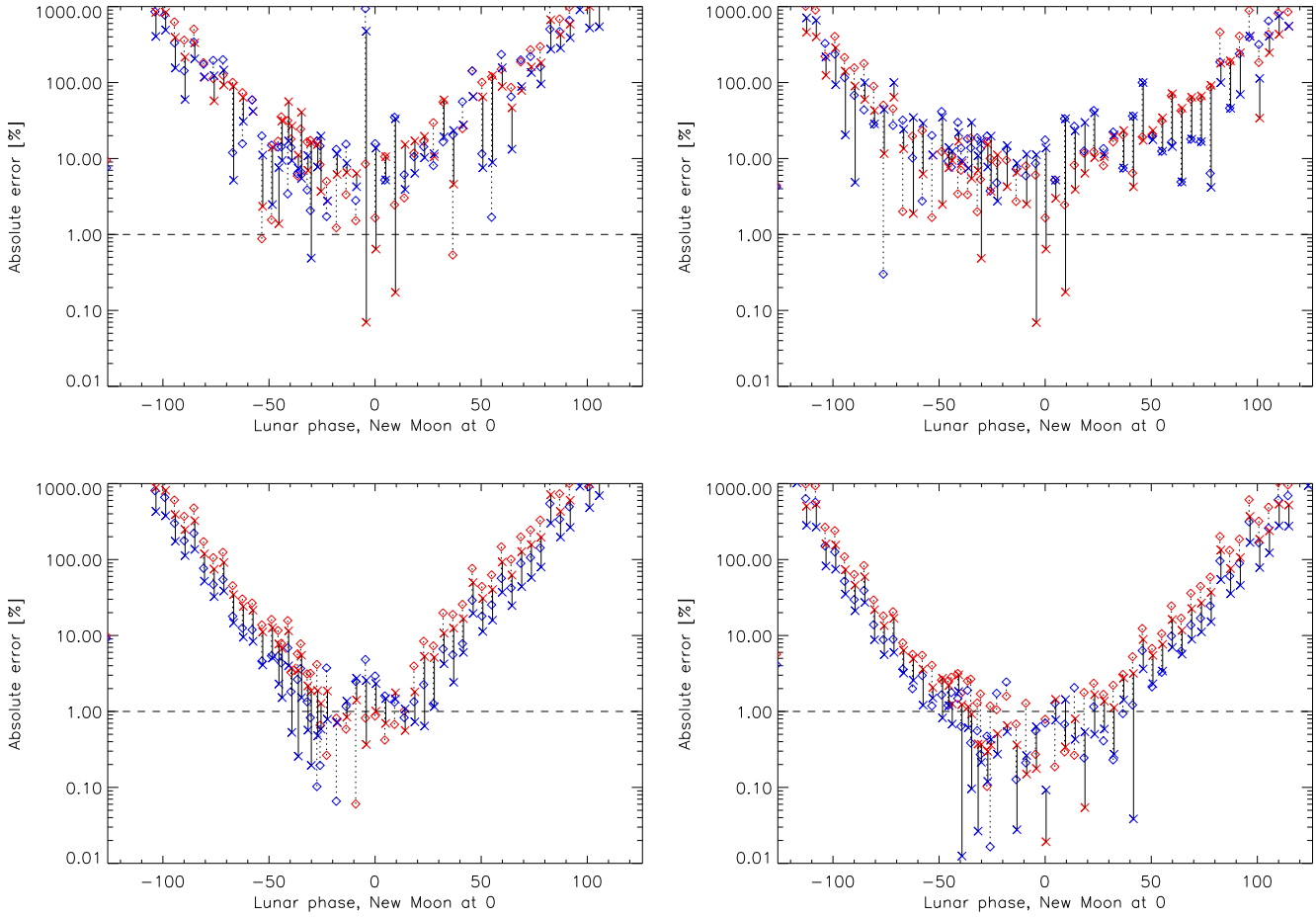

Fig. 2. Test of LINEAR (red symbols) and LOGARITHMIC method (blue) on realistic synthetic images. Absolute percentage errors, calculated from corrected images and the known ideal images are shown. Upper row: A single image with α=-2.56 (left) and -2.88 (right). Crosses show the results at 4/5ths of the disc radius from disc center and diamonds are for 2/3rds from disc centre. Lower row: 100 realistic images co-added. The abscissa shows lunar phase in degrees relative to New Moon at 0. The ordinate shows absolute values only in order to accommodate a few negative percentage errors near lunar phase 0: The sense of the error is primarily such that corrected images carry more flux than is present in the ideal images.

frames available for stacking. We expect that improved methods of alignment, under development, will increase the number of frames available. In addition to reducing the averaged frames we also analyse all single frames. We apply the LINEAR method (see Tables 5 and 7) and the the EFM method (see Tables 4 and 6). For the night of JD 2455858 we show both averaged results from many frames, and results from averaged frames. For JD 2455917 we only show averaged results from single frames. Results from the FFM method will be presented in a future paper.

We see the EFM method, on single images, giving results with standard deviations in the 2 to 5% range, both nights considered. The LINEAR method gives standard deviations that are larger and depend on the night in question: 12–25% S.D. for night 2455858, and 5–9% for night 2455917. In Figure 5 we compare the 5-band photometry for the two methods and nights. On each night the same data reduced with two different methods give similar results. On different nights the earthshine intensity is clearly different in accordance with the expectations for different lunar (and therefore terrestrial) phases.

Table 4. Results from application of EFM method to images observed on JD 2455858. Given are: the filter name, the number of fits used, the mean of the DS to the per pixel mean image flux, the standard deviation of the DS/BS ratio expressed in percent as the mean DS/BS ratio in percent, and the standard deviation of the mean relative to the mean in percent. The last column - 'stack mean' - gives the DS to the per pixel mean flux in the average image.

Filter	N	mean	SD/mean in %	SD_m/mean in %	stack mean
B	90	0.02352	2.2	0.3	0.0222
V	79	0.01798	2.7	0.4	0.0174
VE1	92	0.01729	2.8	0.4	0.0167
VE2	83	0.01612	3.4	0.5	0.0158
IRCUT	99	0.01733	4.1	0.6	0.0159

7. Discussion

We have seen the LINEAR and LOGARITHMIC methods work well on synthetic test images in a narrow range of lunar phases. We have seen how the LOGARITHMIC extends the powers of the LINEAR

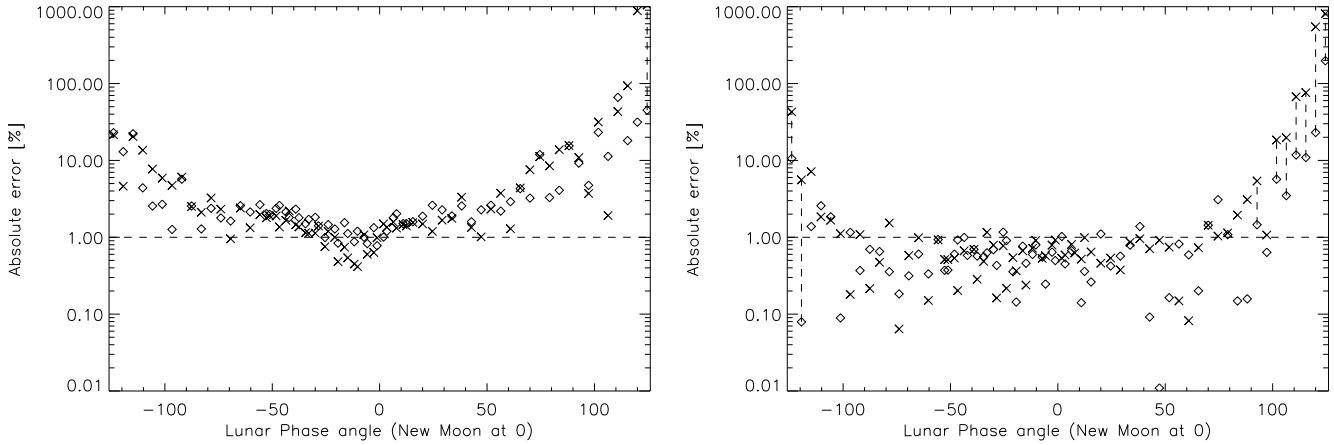

Fig. 3. Empirical forward method tested on synthetic lunar images. At left is the test using synthetic images with α=-2.56 and at right for -2.88. Stacks of 100 coadded images were simulated for every 9 hours in a lunar month. The lunar phase is shown in degrees using New Moon as phase 0. The error is the difference, expressed in percent, between the actual DS intensity and the value in images cleaned with the EFM method. Crosses indicate values from a patch on the image at 4/5ths of the radius from disc center towards the DS rim, and diamonds indicate values in a box at 2/3rds radius from the disc centre. Absolute values of errors are shown.

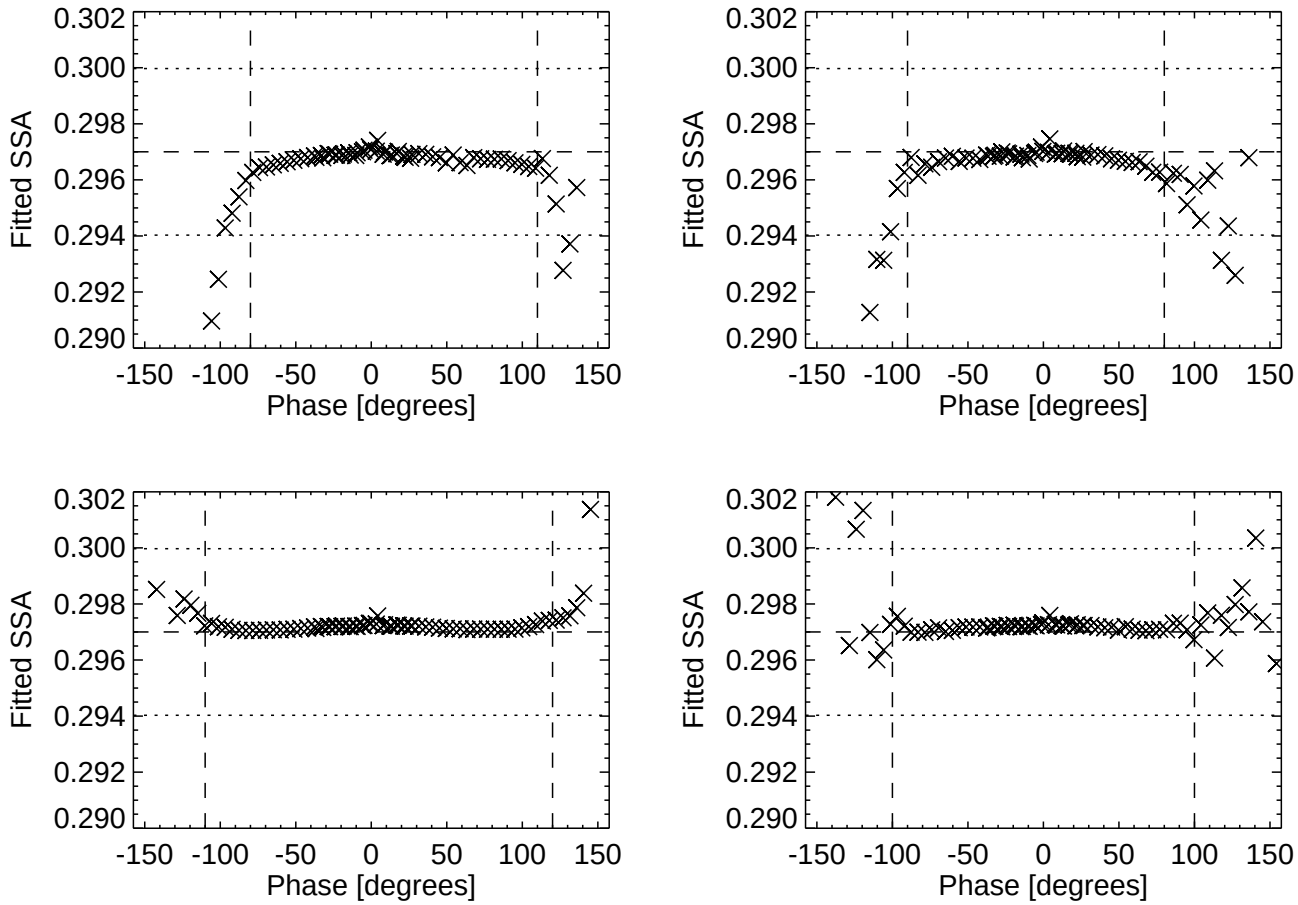

Fig. 4. Full forward method tested on synthetic lunar images. Shown is the value for single scattering albedo retrieved by fitting models to images generated with known settings of the terrestrial albedo. In the top row are results from single images, against lunar phase: New Moon is at phase zero. In the bottom row are results from fitting images that each were the result of co-adding 100 images. The left column is for $\alpha = -2.56$, the PSF parameter which determines the width. In the right column α=-2.88. In all tests the single scattering albedo on the Lambertian-sphere model Earth was 0.297 which is shown as the dashed line. Dotted lines are the 1% limits. Dashed vertical lines show where the results seem to break down and become too noisy.

Table 5. Results from application of the LINEAR method to images observed on JD 2455858.

Filter	N	mean	SD/mean in %	SD_m/mean in %	stack mean
B	90	0.0226	12.5	1.3	0.0227
V	79	0.0178	17.4	2.0	0.0180
VE1	86	0.0165	24.3	2.6	0.0116
VE2	80	0.0164	24.7	2.8	0.0152
IRCUT	99	0.0163	23.7	2.4	0.0164

Table 6. Results from application of EFM method to images observed on JD 2455917. Given are: the filter name, the number of fits used, the mean of the DS to the per pixel mean flux, the standard deviation of the DS/BS ratio expressed in percent as the mean DS/BS ratio in percent, and the standard deviation of the mean relative to the mean in percent.

Filter	N	mean	SD/mean in %	SD_m/mean in %
B	55	0.03502	4.0	0.5
V	44	0.02799	4.2	0.6
VE1	47	0.02744	4.4	0.6
VE2	65	0.02584	3.5	0.4
IRCUT	43	0.02709	3.0	0.5

Table 7. Results from application of the LINEAR method to images observed on JD 2455917.

Filter	N	mean	SD/mean in %	SD_m/mean in %
B	55	0.0367	5.0	0.7
V	45	0.0293	7.5	1.1
VE1	57	0.0269	8.9	1.2
VE2	66	0.0256	5.9	0.7
IRCUT	45	0.0276	5.2	0.8

method, and we have seen the effect of working on high SNR data. We also saw a strong bias for large lunar phases: This is not unexpected as the ES intensity drops as lunar phase increases - the proximity of all DS areas to the wings of the BS halo also increases with lunar phase: Essentially the LINEAR method cannot cope with the halo when it is strong and the reference patch is close to it. We understand the PSF as a power-law entity and understand why these methods have limited applicability for large lunar phases: A power law is first of all not linear with distance to the center; only approximately so at large distances and narrow radial increments - secondly, the LOGARITHMIC method also fails at a slightly larger lunar phase because the method is applied in lin-log space - and a power law is only perfectly linear in log-log space.

The FFM method seems to be the best method of those analyzed: It yields very accurate and precise estimates of the terrestrial albedo. It does so by utilizing virtually all pixels in the image, which leads to a higher quality fit. When DS intensities are reported we have a contribution from spatial variance in the lunar image considered - this increases the reported error: For the tests considered in this paper this is a factor for the EFM method where different levels of spatial smoothing in the synthetic observed image and the ideal source are present. The size of the RMSE bias in Figure 3 is therefore somewhat higher than the actual model-fit error. The smoothness of the albedo results in Figure 4 is impressive, especially compared to the scatter seen for fitted intensities in the other methods' Figures. We ascribe

Fig. 5. Intensities of the DS expressed relative to the BS, for 5 photometric filters, and two nights. The intensity ratios are shown as magnitudes (i.e $-2.5log_{10}$(ratio) with an arbitrary offset added to each filter. The crosses refer to the EFM method, and the boxes to the LINEAR method. Analysis was performed on single images and the results for each filter averaged. See details in Tables 4– 7

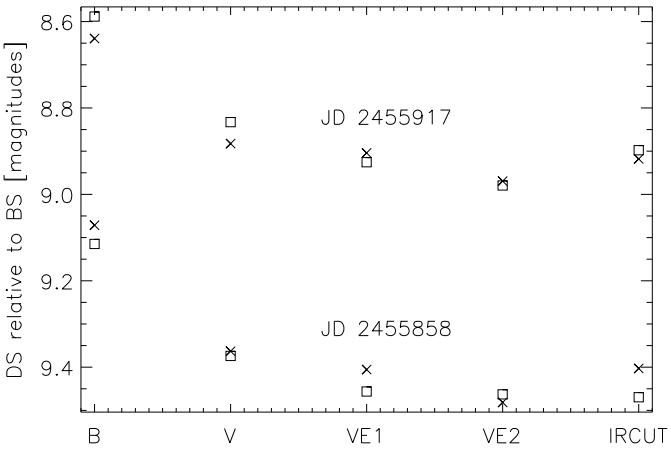

this smoothness to the fact that the FFM extracts a global property from the image, using all the pixels present, while the other methods extract intensities from necessarily rather small areas on the lunar disc.

Another factor explains the performance failure of the LINEAR method at large lunar phases - we do not use an internal occulter and therefore the halo around the BS is present in all our images. The BBSO team has available a separate mechanism that inserts a solid knife edge as an occulter of the BS in the prime focus of their telescope. We speculate, but have seen no published evidence, that the presence of the BBSO-system knife-edge not only reduces the amount of light let into the lower parts of the optical system, but also stops a bright halo being formed in the parts of the optical system between the knife and the CCD. We can conceive of no role for the occulting knife-edge, apart from the mentioned effect on ghost images and diffuse scattering mentioned above, to reduce the formation of a BS halo if this is generated by the atmosphere (as suggested by Goode et al. 2010) or the first passage of light through the main objective. Careful analysis of ray-tracing experiments through a slightly scattering set of secondary optics may be able to cast light on this question, but is beyond the scope of the present investigation. Unquestionably, the BBSO knife-edge reduces internal diffuse reflections after the prime focus.

The LINEAR and LOGARITHMIC methods work directly on observed images and basically only need some fixed-points on the lunar disc - the centre and the radius. The EFM is even easier to use as it requires only an observed image as input. It does, however, require that a choice is made of which BS pixels play the role of source. The EFM method has the advantage that the actual distribution of light on the BS is at hand - in the FFM we have to use a model for this, so we are dependent on how good our lunar reflectance model is.

The FFM models the entire image but requires that the lunar model image is centred and radially scaled appropriately to the observed image. Our synthetic model software takes care of the geometric scaling, but centring on the observed image is required.

When we look at the results from real data we see two significant things: evaluated on data from the same nights the EFM outperforms the LINEAR method in terms of the scatter of the data by a factor of 5 to 6 on the darker of the two nights but only by a factor of about 2 on the earthshine-brighter night – on the brighter night the DS is less bothered by the halo from the BS and the LINEAR method has a better chance of doing well. This is a result in line with the theoretical expectations. However, the EFM does not reach the low levels of standard deviation of the mean promised by the theoretical study: we would need more frames than we have here. The standard deviations of the means are of course smaller for both methods but the EFM would require 9 to 16 times more images to have a standard deviation of the mean which lived up to the results from the tests on synthetic images. We see the results based on stacked and averaged images generally similar to averages of results from single images.

We have investigated the measurement of earthshine intensity using a number of methods. These necessarily involve some choices about how to fit the data in practice. We discuss now some of these choices, the effects they might have, and ideas for further study. In the LINEAR and LOGARITHMIC methods the lunar disc and the sky outside is divided into cones: The width of these cones and their point of convergence are arbitrary choices. We chose the width and the origin of the cones to follow Qiu et al. (2003). Other choices of cone width are certainly possible and it might be useful to start the cones from the BS instead of the centre of the disc. Because the PSF is centrally dominated, although it has wide wings, much of the light just off the lunar disc originates in the disc itself and is overlain by the tail of scattered light from the BS. By going too close to the edge of the disc a small chance of introducing a bias by including the 'upturn' exists - one should therefore try to avoid the pixels closest to the Moon. We exclude the pixels nearer than 7 pixels from the rim. In the EFM an important choice is made when positioning the mask that excludes the lunar disc. It should also start off the lunar disc. We start it 16 pixels off the disc rim. Centring of that mask on the lunar disc, and automatically determining the lunar disc radius affects the quality of the subsequent fit, and we want to return to this issue in future work. At present the lunar rim is detected using edge detection techniques on histogram equalized images. Sobel and Laplacian filters (Langford et al. 2009) were tested and were found to perform similarly on real images. The FFM method has no mask to align but the synthetic image used must be aligned with the observed image: Chiefly because this is a delicate operation we have chosen to postpone discussion of this step and only show results from synthetic images where alignment is not needed. The EFM requires a choice of which pixels to use as the 'source' as discussed above. Both the EFM and the FFM furthermore depend on an offset that is added to images to avoid negative- and zero-valued pixels. Since the *relative* error is minimized the choice of offset influences the objective function to minimize. We have briefly investigated the effect of this on results using synthetic images and find that the best-fit DS/BS ratio does depend on the offset choice. The effect has the nature of a small bias which is a few percent for single images but decreases to the sub-1% level when 100 images are co-added. This implies a biasing dependency on noise in the fitting method. We recommend using the method on co-added images and not relying on co-adding results after single-image analysis despite the encouraging empirical result, above.

8. Summary and Conclusions

We summarize our synthetic-images based test procedures in Table 8. Our extensive tests in this paper have confirmed the error levels for the LINEAR method described in publications – e.g. (Qiu et al. 2003) and Goode et al. (2010). We have shown that without further corrections of the residual scattered light the LINEAR method will always be biased towards too high a DS intensity. We suggest that the LOGARITHMIC method can ameliorate these effects.

We show that the various flavours of forward modelling methods have the potential to produce more precise and less biased ES intensity data for a wider range of lunar phases, up to about 120 degrees from New Moon in the best case. The FFM method even provides high quality terrestrial albedo values directly without further processing - on single images the uncertainty and the bias is near the stated goal of 0.1%, for lunar phases below 40-50 degrees, while these levels triple if 90 degrees of phase is considered. If we stack 100 images the test is able to achieve very low uncertainty and bias even at 90-110 degrees of phase, showing the effect of the SNR on the fitting method.

With the present choice of direct imaging with subsequent stacking of hundreds of images we have shown the ability to improve on the current best methods, and we see potential in future implementation of more complex optical occulting systems. Significantly, we have shown that low levels of bias - as well as scatter - is potentially possible with our forward-modelling methods - which does not appear to be the case for the sky-extrapolation method: This is useful information for future applications of earthshine data in fields where not precision but accuracy in the long term is a factor. In future work we will revisit the issues that we have not touched on here - namely those regarding the relationship between the terrestrial albedo we can derive from earthshine telescopes using our new methods and climate research requirements.

Finally, real images are more complex than our simplistic synthetic images and data quality issues not discussed in this paper come into play: we are encouraged, however, that stacking of images and forward modelling and fitting of observed images reaches the necessary goals during synthetic testing. In combination with an occulting device that lowers the levels of scattered light inside the telescope, and probably helps eliminate part of the halo around the DS, we expect further improvements in quality of results.

Acknowledgements. This work was made possible by a generous grant from the VINNOVA foundation in Sweden who asked for proposals for 'novel climate observing systems' and accepted ours. Additional support from Lund Observatory and the Danish Meteorological Institute is also acknowledged. We would like acknowledge the support of the staff of the NOAA Mauna Loa Observatory.

References

Bernstein, R. A. 2007, ApJ, 666, 663
Chae, J. 2004, Sol. Phys., 221, 15
Darudi, A., Owner-Petersen, M., Thejll, P., et al. 2010, in Society of Photo-Optical Instrumentation Engineers (SPIE) Conference Series, Vol. 7733, Society of Photo-Optical Instrumentation Engineers (SPIE) Conference Series
de Vaucouleurs, G. 1948, Annales d'Astrophysique, 11, 247
de Vaucouleurs, G. 1958, ApJ, 128, 465
Ford, E. B., Seager, S., & Turner, E. L. 2001, Nature, 412, 885
Goode, P. R., Qiu, J., Yurchyshyn, V., et al. 2001, Geophys. Res. Lett., 28, 1671
Goode, P. R., Shoumko, S., Pallé, E., & Montañés-Rodríguez, P. 2010, Advances in Astronomy, 2010
Hapke, B. 1993, Theory of reflectance and emittance spectroscopy (Cambridge, UK: Cambridge University Press)

Table 8. Summary of tests of methods to remove scattered-light, based on synthetic image analysis and modelling.

Method name	Description	Pros	Cons
LINEAR	Subtraction of scattered light, extrapolated onto the lunar disc from the sky brightness. Based on linear images. Corrected DS **intensities as output**. Performance improves towards sky edge of the DS. Co-adding many images reduces noise. Works best near New Moon. Can yield errors below 1% up to 40 degrees from New Moon, in best case.	Simple, entirely empirical.	Increasing bias as phase grows. Terrestrial reflectance model needed to convert earthshine intensities to terrestrial albedo.
LOGARITHMIC	Like LINEAR but is applied to logarithms of images. Corrected DS **intensities as output**.	Outperforms LINEAR by another 10 degrees of phase in high SNR images.	Terrestrial reflectance model required.
EFM	Forward modelling and fitting of model image to the sky part of the observed image. Uses bright parts of the observed image as a source term for calculating the model image. Data on the DS intensity is extracted from the difference between the observed image and the best-fitting model image. Corrected DS **intensities as output**.	Works from observed images, avoiding alignment issues and reflectance modelling.	Choice of source region required. Computationally intensive. Terrestrial reflectance model required.
FFM	Forward modelling of entire Moon based on synthetic images of the Moon exposed to ES from a model Earth. Terrestrial **albedo directly as output**.	Can produce albedo data to +/- 90 degrees of lunar phase from single images. +/- 120 from 100-image stack of images. Bias is $\leq$1/5% and the scatter is $\leq$.1 %. For 100 co-added images the bias and scatter is much smaller.	Lunar and terrestrial reflectance model required. Computationally intensive.

Hapke, B. W. 1963, J. Geophys. Res., 68, 4571
Jensen, H. W., Durand, F., Dorsey, J., et al. 2001, in Proceedings of the 28th annual conference on Computer graphics and interactive techniques, SIGGRAPH '01 (New York, NY, USA: ACM), 399–408
Johannes & Mueller. 1997, Advances in Space Research, 19, 1307
King, I. R. 1971, PASP, 83, 199
Langford, S. V., B. Wyithe, J. S., & Turner, E. L. 2009, Astrobiology, 9, 305
Manalo-Smith, N., Smith, G. L., Tiwari, S. N., & Staylor, W. F. 1998, J. Geophys. Res., 103, 19733
Markwardt, C. B. 2009, in Astronomical Society of the Pacific Conference Series, Vol. 411, Astronomical Data Analysis Software and Systems XVIII, ed. D. A. Bohlender, D. Durand, & P. Dowler, 251
Oakley, P. H. H. & Cash, W. 2009, ApJ, 700, 1428
Owner-Petersen, M., Andersen, T., Ardeberg, A., Thejll, P., & Gleisner, H. 2008, in Society of Photo-Optical Instrumentation Engineers (SPIE) Conference Series, Vol. 7012, Society of Photo-Optical Instrumentation Engineers (SPIE) Conference Series
Pallé, E., Goode, P. R., & Montañés-Rodríguez, P. 2009, Journal of Geophysical Research (Atmospheres), 114, D00D03
Qiu, J., Goode, P. R., Pallé, E., et al. 2003, Journal of Geophysical Research (Atmospheres), 108, 4709
Racine, R. 1996, PASP, 108, 699
Robinson, M. & Riner, M. 2005, Journal of Earth System Science, 114, 669
Stephens, G. L., Campbell, G. G., & Vonder Haar, T. H. 1981, J. Geophys. Res., 86, 9739
Stone, T. C. 2008, in Society of Photo-Optical Instrumentation Engineers (SPIE) Conference Series, Vol. 7081, Society of Photo-Optical Instrumentation Engineers (SPIE) Conference Series
Yu, J., Ryu, D.-O., Ahn, S.-H., & Kim, S.-W. 2011, in Society of Photo-Optical Instrumentation Engineers (SPIE) Conference Series, Vol. 8146, Society of Photo-Optical Instrumentation Engineers (SPIE) Conference Series

[1] Danish Climate Centre, DMI, Lyngbyvej 100, DK-2100 Copenhagen Ø, Denmark
e-mail: pth@dmi.dk
[2] Turko Observatory, Finland
e-mail: cflynn@utu.fi
[3] Lund Observatory, Lund University, Sweden
e-mail: hes@dmi.dk
[4] School of Astronomy, Institute for Research in Fundamental Sciences, Tehran, Iran